



Spectroscopy of Magnesium Sulfate Double Salts and Their Implications for Mars Exploration

Erbin Shi [†], Ruize Zhang [†], Xiaojia Zeng, Yanqing Xin ^{*†} , Enming Ju and Zongcheng Ling

Shandong Key Laboratory of Optical Astronomy and Solar-Terrestrial Environment, School of Space Science and Physics, Institute of Space Sciences, Shandong University, Weihai 264209, China; erbinshi@sdu.edu.cn (E.S.); 202317810@mail.sdu.edu.cn (R.Z.); zengxiaojia@mail.gyig.ac.cn (X.Z.); 202121031@mail.sdu.edu.cn (E.J.); zcling@sdu.edu.cn (Z.L.)

* Correspondence: yqxin@sdu.edu.cn; Tel.: +86-15154030811

[†] These authors contributed equally to this work.

Abstract: Magnesium sulfate has been widely detected on the surface of Mars. The occurrence of magnesium sulfate and mixed cationic sulfates preserves clues regarding the sedimentary environment, hydrological processes, and climate history of ancient Mars. In this study, seven magnesium sulfate double salts were synthesized in the laboratory using a high-temperature solid phase reaction or slow evaporation of aqueous solutions. The samples were analyzed using X-ray diffraction to confirm their phase and homogeneity. Subsequently, the Raman, mid-infrared spectra, and visible near-infrared spectra of these samples were collected and analyzed. Our results showed that the spectra of the analyzed magnesium sulfate double salts exhibited distinctive spectral features. These laboratory results may provide new insights for the identification of various magnesium sulfate double salts on Mars during the interpretation of in situ data collected by Scanning Habitable Environments with Raman and Luminescence for Organics and Chemicals (SHERLOC), SuperCam, and the ExoMars Raman Laser Spectrometer (RLS). In addition, the MIR and VNIR spectra features obtained in this study provide an improved reference and spectra library for decipherment of data sourced from the Thermal Emission Spectrometer (TES), Thermal Emission Imaging System (THEMIS), and Mars Mineralogical Spectrometer (MMS).

Keywords: Mineralogy; Spectroscopy; Mg-sulfates; double salts; Mars



Citation: Shi, E.; Zhang, R.; Zeng, X.; Xin, Y.; Ju, E.; Ling, Z. Spectroscopy of Magnesium Sulfate Double Salts and Their Implications for Mars Exploration. *Remote Sens.* **2024**, *16*, 1592. <https://doi.org/10.3390/rs16091592>

Academic Editors: Roberto Orosei, Giancarlo Bellucci and Kaichang Di

Received: 22 February 2024

Revised: 19 April 2024

Accepted: 28 April 2024

Published: 30 April 2024



Copyright: © 2024 by the authors. Licensee MDPI, Basel, Switzerland. This article is an open access article distributed under the terms and conditions of the Creative Commons Attribution (CC BY) license (<https://creativecommons.org/licenses/by/4.0/>).

1. Introduction

Sulfate minerals (Mg-, Fe-, and Ca-sulfates) have been widely identified across various regions on the Martian surface. The first detection of magnesium sulfate on Mars can be traced back to the Viking spacecraft in 1976. During this mission, the identification of kieserite was proposed based on the correlation between magnesium and sulfur observed in X-ray fluorescence data [1,2]. Subsequently, magnesium sulfate on Mars was identified by OMEGA (Observatoire pour la Minéralogie, l'Eau, les Glaces et l'Activité) and CRISM (Compact Reconnaissance Imaging Spectrometer of Mars Reconnaissance Orbiter) at Arabia Terra, Meridiani Planum, Valles Marineris, Candor Chasma, East Candor, Melas Chasma, Ophir Chasma, and Gale Crater [3–11]. Furthermore, in situ detections have also confirmed the presence of magnesium sulfate at various locations on Mars, including Meridiani Planum, Gusev Crater, and Gale Crater, by the Opportunity, Spirit, and Curiosity rovers, respectively [12–14]. In particular, the presence of $\text{MgSO}_4 \cdot 4\text{H}_2\text{O}$ was confirmed at the Gale Crater [15]. Among the identified phases, kieserite stands out as the most common phase of magnesium sulfate identified on Mars, occasionally associated with calcium sulfates ($\text{CaSO}_4 \cdot n\text{H}_2\text{O}$) [16]. The magnesium sulfates found in various regions on Mars are acknowledged to play a crucial role in the climate evolution and hydrological cycle of Mars, especially because they hold information about different environmental parameters (e.g., pH, Eh, and salinity) [14,17].

Sulfate has also been observed to occur as light-toned veins in the Gale Crater, Jezero Crater, and Endeavor Crater [18–21]. The predominant phases in these light veins have primarily been identified as calcium sulfates exhibiting varying degrees of hydration, including anhydrite, bassanite, and gypsum [18–21]. This reveals the fluid process and the environmental evolution of typical regions on Mars. However, based on APXS (Alpha Particle X-ray Spectrometer) and LIBS (Laser-Induced Breakdown Spectroscopy) measurements, the composition of these light veins is complex. CaO and SO₃ cannot be balanced in these veins; in addition to Ca²⁺, they also contain other cations, such as Mg²⁺, K⁺, Na⁺, and Fe³⁺ [19–21]. This phenomenon is not limited to calcium sulfate veins; magnesium sulfate bedrock enrichments have also been observed in a relatively thin (<10 m) stratigraphic interval within the heterolithic Sutton Island member in the Gale Crater. Interestingly, discrepancies in the balance between SO₃ and MgO have been noted in this context [14]. Furthermore, in the Gale Crater, the concentrations of the Ca²⁺, Na⁺, Mg²⁺, and K⁺ cations in amorphous materials are also not sufficient to entirely balance the abundance of SO₄²⁻ [22]. The APXS data obtained from the Mars Exploration Rover (MER) Opportunity highlighted an association of Ca-sulfate with Mg-sulfate in the sedimentary outcrops of the Meridiani Planum [23], along with the UV-vis data from the OMEGA spectrometer on Mars Express [16]. These observations suggest the presence of mixed cations (e.g., double salts and solid solutions) on Mars.

Regarding the origin of magnesium sulfate double salts or solid solutions, previous works have suggested that the sulfur may be sourced from various fluid activities on Mars. These include high-temperature volcanic gases, hydrothermal fluids [24–26], or low-temperature groundwater interacting with S-bearing rocks. In addition, modeling studies have been used to understand the nature and sequence of salts precipitated from multicomponent magnesium-sulfur-rich solutions [27]. These models aim to serve as potential analogs for the overall composition of the early Martian hydrosphere [27–29]. For example, King et al. (2004) predicted phases in the Mg-Na-SO₄-Cl system based on groundwater compositions of igneous rocks [27]. These groundwaters were found to be enriched in Mg, Ca, Na, K, SO₄, HCO₃/CO₃, and Cl. The evolution of these groundwaters, which should be acidic and sulfate-rich [30], has been predicted to form different double salts or solid solutions [27]. Specifically, blödite (Na₂Mg(SO₄)₂·4H₂O) is an important phase in the Mg-Na-SO₄-Cl system, and picromerite (K₂Mg(SO₄)₂·6H₂O) is another important phase in the low calcium alkali water and salt system [27].

To date, the presence of magnesium sulfate double salts on Mars is still being debated. To accurately reveal the mineralogy of light-toned veins and magnesium sulfate sedimentary rocks, seven magnesium sulfate double salts were synthesized in the laboratory. The synthesized samples were divided into Na-Mg, K-Mg, and K-Ca-Mg systems. XRD (X-ray diffraction), Raman, MIR (mid-infrared), and VNIR (visible and near-Infrared) spectrometers were used to analyze these samples. The distinctive spectral features identified in this analysis aim to fill the existing gap in the spectral understanding of magnesium sulfate double salts. Our results are expected to be instrumental in processing remote sensing and in situ data, and in detecting magnesium sulfate double salts on Mars and Earth. Eventually, this work can also provide laboratorial parameters for constraining the formation and alteration processes of magnesium sulfate double salts on Mars.

2. Materials and Methods

2.1. Materials

Seven magnesium sulfate double salts were synthesized in the laboratory using high-temperature solid phase reaction or slow evaporation of aqueous solution methods. The reagents used in this study included sodium sulfate (Na₂SO₄, ≥99%, AR (Analytical Reagent)), anhydrous sodium sulfate (MgSO₄, ≥99%, AR), potassium sulfate (K₂SO₄, ≥99%, AR), magnesium sulfate heptahydrate (MgSO₄·7H₂O, ≥99%, AR), and calcium sulfate dihydrate (CaSO₄·2H₂O, ≥99%, AR). The CaSO₄·2H₂O, Na₂SO₄, MgSO₄, K₂SO₄, and MgSO₄·7H₂O were all analytical reagent phases, purchased from the Sinopharm Chemical Reagent Beijing Co., Ltd. (Beijing, China).

2.2. Synthesis of Magnesium Sulfate Double Salts

Blödite ($\text{Na}_2\text{Mg}(\text{SO}_4)_2 \cdot 4\text{H}_2\text{O}$) was synthesized by evaporating salt solutions that contained 18.18 wt% of sodium sulfate (Na_2SO_4) and 16 wt% of anhydrous magnesium sulfate (MgSO_4) at 323 K in an oven for 5 days [31].

Konyaite ($\text{Na}_2\text{Mg}(\text{SO}_4)_2 \cdot 5\text{H}_2\text{O}$) was prepared by evaporating solutions containing sodium sulfate (Na_2SO_4) and magnesium sulfate heptahydrate ($\text{MgSO}_4 \cdot 7\text{H}_2\text{O}$) in a molar ratio of 1:1 in a Petri dish at 308 K for 5 days in an oven [32].

Löweite ($\text{Na}_{12}\text{Mg}_7(\text{SO}_4)_{13} \cdot 15\text{H}_2\text{O}$) was synthesized from a solution of magnesium sulfate heptahydrate ($\text{MgSO}_4 \cdot 7\text{H}_2\text{O}$) and anhydrous sodium sulfate (Na_2SO_4) in a molar ratio of 7:6 at 353 K for 5 days in an oven [33].

Langbeinite ($\text{K}_2\text{Mg}_2(\text{SO}_4)_3$) was synthesized using magnesium sulfate heptahydrate ($\text{MgSO}_4 \cdot 7\text{H}_2\text{O}$) and anhydrous potassium sulfate (K_2SO_4) which was mixed according to a molar ratio of 2:1 [34], and ground for 1 h. The ground materials were put into a muffle furnace, heated at 973 K for 3 h, and then removed immediately and placed at room temperature to quench. The quenched product was ground for 20 min, then heated again at 673 K for about 24 h. The product was immediately placed at room temperature, left to cool, and then bottled.

Leonite ($\text{K}_2\text{Mg}(\text{SO}_4)_2 \cdot 4\text{H}_2\text{O}$) was synthesized by mixing 0.015 mol anhydrous potassium sulfate (K_2SO_4) and 0.015 mol magnesium sulfate heptahydrate ($\text{MgSO}_4 \cdot 7\text{H}_2\text{O}$) in 70 mL H_2O , followed by blending the solution in a magnetic mixer for 30 min. Then, water from the solution was evaporated in a drying oven at 363 K [35]. Three days later, the crystal was obtained under the experimental conditions and bottled.

Picromerite ($\text{K}_2\text{Mg}(\text{SO}_4)_2 \cdot 6\text{H}_2\text{O}$) was synthesized using an equal molar amount of anhydrous potassium sulfate (K_2SO_4) and magnesium sulfate heptahydrate ($\text{MgSO}_4 \cdot 7\text{H}_2\text{O}$) in a triple distilled water medium. The resulting mixture underwent evaporation to remove water in a drying oven at 308 K [36]. After four days, the water had evaporated completely, and the crystal was harvested.

$\text{K}_2\text{CaMg}(\text{SO}_4)_3$ was synthesized by mixing anhydrous potassium sulfate (K_2SO_4), magnesium sulfate heptahydrate ($\text{MgSO}_4 \cdot 7\text{H}_2\text{O}$), and calcium sulfate dihydrate ($\text{CaSO}_4 \cdot 2\text{H}_2\text{O}$) in equal molar amounts. The mixture was ground for 45 min. Then, the ground material was put into a muffle furnace, heated at 1073 K for 20 h, and then cooled to room temperature. The cooled product was ground for half an hour, heated at 673 K for 17 h, and then slowly cooled to room temperature. This synthesis method comes from PDF#20-0866 [37].

2.3. Instruments

XRD analysis was carried out at Shandong University, Weihai, utilizing a Rigaku UltimaIV diffractometer equipped with $\text{CuK}\alpha$ radiation ($\lambda = 1.54052 \text{ \AA}$). The measurements were conducted at an acceleration voltage of 40 kV, a current of 40 mA, and a scanning step of 0.02° , within the range of 5° to 70° . The software JADE 6.5, along with the PDF-2004 database from Materials Data Inc. (Greensburg, PA, USA), was employed to determine the position and width of the diffraction peaks, as well as the crystal face index.

The homogenous and phase identification of the seven synthesized samples was carried out using Raman spectroscopy. The Raman spectra of the magnesium sulfate double salts were obtained using the InVia Raman imaging system of Renishaw's micro laser Raman spectrometer. A 532 nm laser excitation from a DPSS laser and a $50\times$ telephoto objective was used to collect signals. The Raman spectra of the samples were collected in the range of $100\text{--}4000 \text{ cm}^{-1}$, including basic molecular and lattice vibration modes. The spectral resolution of the InVia system was better than 1 cm^{-1} , and the spectral repeatability was $\pm 0.2 \text{ cm}^{-1}$. The emission line of the Ne lamp was used to calibrate the wavelength of the spectrometer, and also to calibrate the Raman peak position of the Si chip at $\sim 520.7 \text{ cm}^{-1}$ every day. Through these two calibrations, an accuracy of $\pm 0.2 \text{ cm}^{-1}$ was ensured for the Raman peak position.

The Bruker vertex 70 Fourier Transform infrared spectrometer at Shandong University in Weihai was used to obtain the MIR spectra of samples in the range of $400\text{--}4000 \text{ cm}^{-1}$

with 32 scans. The Spectral resolution was better than 0.16 cm^{-1} , with a signal-to-noise ratio of 45000:1. To measure the MIR transmission spectrum, we chose the HF-12 tablet mold. The KBr and sample were mixed at a mass ratio of 100:1, then the mixture was ground. Finally, the ground mixture was put into the HF-12 tablet mold and pressed by the tablet press at 12–13 MPa for 2 min.

The FiledSpec4 Hi-Res VNIR spectroradiometer (Analytical Spectral Devices (ASD), Inc. (Boulder, CO, USA)) at Shandong University in Weihai was used to obtain the VNIR spectra of the samples in the range of 350–2500 nm. The spectrum had a resolution of 3 nm in the range of 350–1000 nm and 8 nm in the range of 1000–2500 nm. Before measurement, the spectrometer was calibrated using a Lambert surface (SRS-99-010) from Labsphere® (Peabody, MA, USA).

3. Results

3.1. XRD Pattern

The XRD patterns collected from the synthesized seven magnesium sulfate double salts are shown in Figure 1. All samples were not ground, and were measured at room temperature with a 2θ angle of 5° – 70° . The seven samples were then directly put into the molds and the surfaces were flattened. The phase identifications of the seven samples were firstly conducted by XRD, according to the standard in the PDF-2004 mineral database. The diffraction patterns of these samples were well matched with those of the PDF-2004 mineral database according to evaluation of the positions of all of the apparent peaks. The results indicated that the synthesized samples were pure and homogeneous. Consequently, we were able to proceed with additional spectroscopic analyses of the pure synthesized samples.

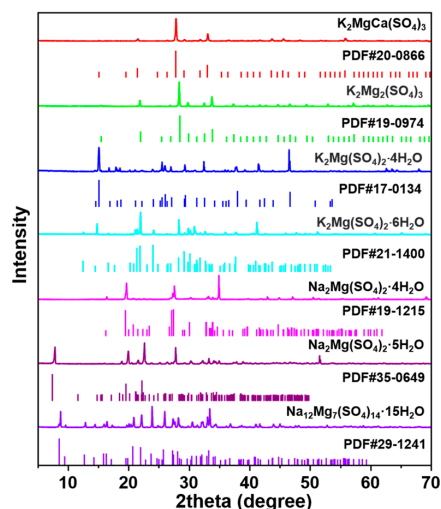


Figure 1. XRD patterns of seven synthesized magnesium sulfate double salts in the region between 5° and 70° . The XRD patterns of these double salts were well matched with the PDF-2004 database, indicating that the samples were prepared successfully.

3.2. Raman

All of the samples were placed on a slide without grinding and then pressed flat, and testing was carried out at room temperature, with the laser shining vertically at the sample. The characteristic Raman spectra of the seven magnesium sulfate double salts were collected from 100 to 4000 cm^{-1} (Figure 2; Table 1). The Raman spectra revealed the fundamental vibrational modes of the molecules. The vibrational characteristics of the synthesized samples in the region of 100 – 1400 cm^{-1} indicated the effects of SO_4^{2-} tetrahedra, including symmetric stretching (ν_1), antisymmetric stretching (ν_3), symmetric bending (ν_2), and antisymmetric bending (ν_4) modes around 983, 1105, 450, and 611 cm^{-1} , respectively [38,39]. The region between 1500 and 4000 cm^{-1} showed the O–H stretching

mode of the structure of H₂O. H₂O characteristics relating to the symmetric stretching (ν_1), antisymmetric stretching (ν_3), and bending (ν_2) modes were typically observed at around 3450, 3615, and 1640 cm⁻¹, respectively [38,39]. The Raman features, and their assignment to the seven synthesized samples, are summarized in Table 1.

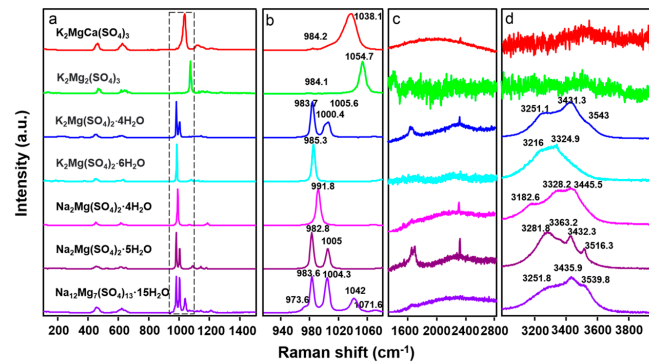


Figure 2. Raman spectra of seven magnesium sulfate double salts. (a) The 100–1400 cm⁻¹ region, which indicates the effects of SO₄²⁻ tetrahedra. (b) The enlarged view of the area framed by dotted lines. (c) The 1500–2850 cm⁻¹ region, which indicates the effects of water bending vibrations. (d) The 3000–4000 cm⁻¹ region, which indicates the effects of water stretching vibrations. All of these have distinct Raman features that can be used to identify them on Mars and Earth.

Compared with previous studies, the Raman features of Na₂Mg(SO₄)₂·4H₂O revealed here showed two more peaks at 617.4 cm⁻¹ (ν_4) and 1173 cm⁻¹ (ν_3), and the other peaks exhibited differences of about 3 cm⁻¹ [33]. We assigned these peaks using the H₂O mode assignment of other magnesium sulfate salts [33,38,40], since the Raman measured by Vargas Jentzsch et al. (2011) did not identify peaks in the 1500–4000 cm⁻¹ range [33]. The peaks at 3186.3, 3328.2, and 3445.5 cm⁻¹ were attributed to the H₂O stretching mode, and the weak band at 2329.0 cm⁻¹ was attributed to the H₂O bending mode combined with the rocking mode [38]. The bending modes at about 1640 cm⁻¹ were too weak to be observed.

Several peaks were also observed in the corresponding positions of the ν_1 mode, ν_2 mode, ν_3 mode, and ν_4 mode in other samples. The strong peaks of the ν_1 mode were consistent with previous work, but the positions and numbers of some peaks were not particularly compatible with past research. For Na₂Mg(SO₄)₂·5H₂O, the ν_4 mode had three peaks at 613.9, 622.8, and 650.1 cm⁻¹, which was different from the four peaks observed at 602, 610, 619, and 648 cm⁻¹ in a previous study [33]. The ν_3 mode had four peaks at 1090.3, 1130.6, 1145.1, and 1180.1 cm⁻¹, but previous work reported only three peaks at 1091, 1144, and 1179 cm⁻¹ [33]. The observed variations in the Raman feature numbers of Na₂Mg(SO₄)₂·5H₂O between the study by Vargas Jentzsch et al. in 2011 and our results may be attributed to the diverse synthesis methods employed in their production. Different synthetic techniques can yield distinct levels of crystallinity in samples, contributing to the observed differences in their Raman spectra [33]. For Na₁₂Mg₇(SO₄)₁₃·15H₂O, the ν_3 mode had one more peak, located at 1184.9 cm⁻¹, than was detected in previous work. For K₂Mg₂(SO₄)₃, we compared the observed Raman features with the corresponding R070285 from the RRUFF database (rruff.info), and the peak locations matched well with the results in the database. For K₂Mg(SO₄)₂·4H₂O and K₂CaMg(SO₄)₃, we did not find a detailed Raman spectral study. However, the results of XRD showed that the phase of our sample corresponded well with the corresponding PDF reference pattern; thus, the results for these two samples were recognized as accurate. The Raman features of K₂Mg(SO₄)₂·6H₂O were also well matched with the results of Marzougui et al. (2015) [41].

Table 1. Raman peak position (cm^{-1}) of seven magnesium sulfate double salts.

Sample	H ₂ O Mode			SO ₄ Vib. Mode				Others
	Stretching	Bending	Bending + Rocking	ν_1	ν_2	ν_3	ν_4	Lattice Vibration
K ₂ MgCa(SO ₄) ₃				984.2	452.9	1122.8	609.0	
				1025.9	466.0	1154.7	625.4	
				1038.1		1212.4	643.5	
K ₂ Mg ₂ (SO ₄) ₃						1235.8		
				984.1	441.8	1109.1	606.8	128.2
				1054.7	457.4	1124.2	618.2	139.5
					467.7	1136.8	628.0	183.0
					473.8	1151.3	640.0	202.3
						1162.8	658.5	
						1178.1		
K ₂ Mg(SO ₄) ₂ ·4H ₂ O						1197.0		
						1251.1		
	3251.1	1658.8	2329.9	983.7	447.1	1068.7	582.2	105.8
	3431.3			1000.4	456.5	1063.6	604.7	115.8
	3543.0			1005.6	465.5	1116.1	627.0	123.4
						1130.5		131.9
						1145.5		138.0
						1179.7		144.0
								160.5
								205.7
K ₂ Mg(SO ₄) ₂ ·6H ₂ O								220.8
								244.7
	3216.0			985.3	448.0	1080.3	612.0	343.6
	3324.9				460.4	1110.7	632.7	116.8
						1125.8		139.2
						1155.2		187.2
Na ₂ Mg(SO ₄) ₂ ·4H ₂ O								227.9
								270.4
	3182.6		2329.0	991.8	454.9	1069.1	617.4	303.9
	3328.2				470.4	1114.6	629.2	377.4
	3445.5					1173.1		107.1
						1188.1		126.5
								152.2
								181.2
								197.3
								220.9
Na ₂ Mg(SO ₄) ₂ ·5H ₂ O								260.8
								299.1
	3281.8		2328.9	982.8	448.8	1090.3	613.9	351.6
	3363.2			1005.0	458.7	1130.6	622.8	106.0
	3432.3				472.4	1145.1	650.1	122.4
	3516.3					1180.1		145.6
Na ₁₂ Mg ₇ (SO ₄) ₁₃ ·15H ₂ O								170.2
								194.9
	3251.8	1653.3	2152.3	973.6	456.5	1071.6	608.9	217.8
	3435.9			983.6	463.6	1120.5	626.2	242.0
	3539.8			1004.3	473.3	1145.2	642.7	254.4
				1042.0		1184.9		119.5
						1212.3		141.0
							167.2	
							178.6	
							205.3	
							219.3	
							240.6	

3.3. MIR

For MIR spectra measurement, small samples were taken directly from all samples without grinding. Section 2 of this paper describes the sample preparation process. The test was carried out at room temperature, and the sample surface was at a 90-degree angle with the infrared laser (that is, the test angle was 90 degrees). The MIR spectra were taken to support the Raman spectra, and the MIR vibration modes of the seven magnesium sulfate double salts were identified. The peak centers and assignments of the seven synthesized samples are shown in Table 2, and their MIR spectra are shown in Figure 3. Generally speaking, the MIR peak positions were close to the Raman peaks, but the MIR peaks were wider than the Raman ones [38,42]. The MIR spectra characteristics were mainly observed at 350–1300 cm^{-1} , 1500–2000 cm^{-1} , and 3000–4000 cm^{-1} . Among them, 350–1300 cm^{-1} represented the vibration features of the tetrahedron of SO_4^{2-} , while the 1500–2000 cm^{-1} and 3000–4000 cm^{-1} both indicated the spectra features of the H₂O modes [38,39,43]. The ν_1 mode of SO_4^{2-} was the strongest peak in the Raman spectra; however, the ν_1 feature in the mid-infrared spectra data we obtained was not obvious, and there may even have been one

or two less than the ν_1 peak in the Raman data. In the MIR spectra for our samples, the ν_3 mode of SO_4^{2-} contributed the strongest MIR peak. For $\text{K}_2\text{CaMg}(\text{SO}_4)_3$ and $\text{K}_2\text{Mg}_2(\text{SO}_4)_3$, the features that appeared in the regions at $1500\text{--}2000\text{ cm}^{-1}$ and $3000\text{--}4000\text{ cm}^{-1}$ were from adsorbed water [39,44].

Table 2. MIR peak position (cm^{-1}) and assignment of seven magnesium sulfate double salts.

Sample	H ₂ O Mode			SO ₄ Vib. Mode			
	Stretching	Bending	Vibrational	ν_1	ν_2	ν_3	ν_4
$\text{K}_2\text{MgCa}(\text{SO}_4)_3$					417.9	1024.5	612.0
					423.3	1123.5	632.2
$\text{K}_2\text{Mg}_2(\text{SO}_4)_3$				1046.5	442.1		654.4
					415.6	1116.8	605.5
					426.4	1128.5	610.5
					437.1	1139.0	636.4
					448.1	1149.8	660.2
$\text{K}_2\text{Mg}(\text{SO}_4)_2 \cdot 4\text{H}_2\text{O}$	3180.9	1604.0	773.2	981.9	428.9	1090.2	568.4
	3365.9	1676.5	823.1	1003.0	437.5	1114.6	623.5
	3447.6				452.3	1129.4	644.7
	3524.5				477.0	1149.3	668.0
	3558.5				515.6	1169.3	714.7
$\text{K}_2\text{Mg}(\text{SO}_4)_2 \cdot 6\text{H}_2\text{O}$	3187.5	1673.7	761.5	983.1	443.4	1077.0	584.6
	3497.9		875.8		444.7	1160.0	609.1
					456.9	1209.2	632.8
					513.6		705.6
					423.5	1079.0	584.0
$\text{Na}_2\text{Mg}(\text{SO}_4)_2 \cdot 4\text{H}_2\text{O}$	3185.4	1596.5	834.9	993.3	441.1	1116.9	620.4
	3460.6	1631.8	881.8		459.5	1160.5	662.3
		1675.8			466.1	1185.9	725.8
					474.5		
$\text{Na}_2\text{Mg}(\text{SO}_4)_2 \cdot 5\text{H}_2\text{O}$	3219.8	1673.8	761.6	981.8	429.3	1080.8	573.5
	3443.7		825.6	1003.5	444.6	1130.2	603.9
	3516.5				456.1	1148.8	623.5
	3525.3				475.4	1186.7	644.6
	3562.0				480.4		668.0
$\text{Na}_{12}\text{Mg}_7(\text{SO}_4)_{13} \cdot 15\text{H}_2\text{O}$	3205.4	1660.1	773.9	983.8	516.2	1085.5	589.3
	3425.9			997.7	406.4	1119.7	615.7
	3574.6				418.4	1148.1	640.0
					451.2	1184.6	663.9

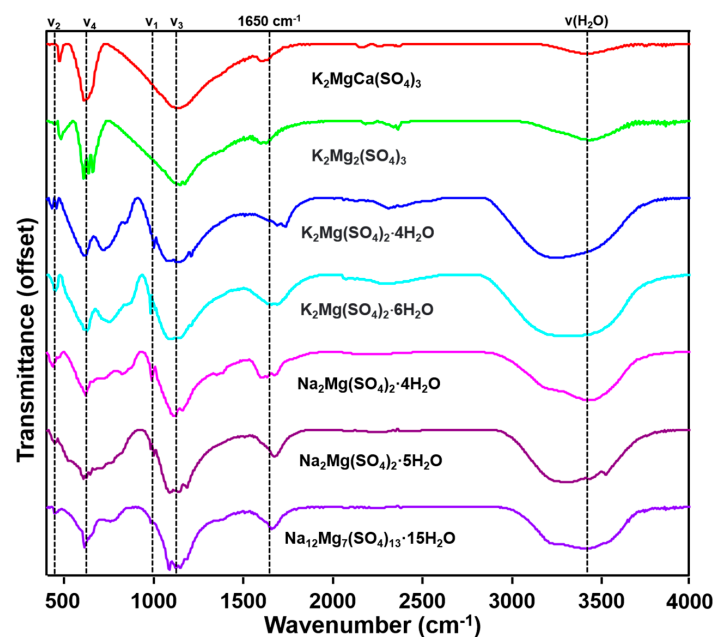


Figure 3. MIR spectra of seven magnesium sulfate double salts. Like Raman spectra, all synthesized samples have distinct MIR features that provide the reference data for TES and THEMIS to identify them on Mars.

3.4. VNIR

For VNIR testing, the samples were also not ground, but were poured directly into the sample pool on the cup light source at room temperature. The light source was at a 30-degree angle to the sample surface. As there were almost no absorption peaks in the VNIR spectra of $\text{K}_2\text{CaMg}(\text{SO}_4)_3$ and $\text{K}_2\text{Mg}_2(\text{SO}_4)_3$, the VNIR spectra from 350 to 2500 nm of the other five hydration samples were taken to investigate the overtone and combination vibrational modes from the H_2O , OH^- , and SO_4^{2-} ionic groups. The 500 to 2500 nm region is displayed in Figure 4. The VNIR spectra of the five assessed magnesium sulfate double salts in this study were similar to the VNIR spectra of magnesium sulfates. For $\text{K}_2\text{Mg}(\text{SO}_4)_2 \cdot n\text{H}_2\text{O}$ ($n = 4, 6$), the peak pattern in the VNIR was very similar, except for a deeper variation in absorption depth with higher hydration, and some peak positions in the high hydrous region showed a small shift to lower wavelengths. The bands between 1700 and 1850 nm were attributed to the combinations of H_2O and OH^- bending, translation, and rotation, and the 2100–2500 nm bands were ascribed to the combinations of H_2O and OH^- and the fundamental overtones of S–O bending [43]. The peaks between 1900 and 2100 nm were attributed to H_2O interacting with the sulfate ion [5]. Other observable features between 900 and 1900 nm were the overtones and combinations of O–H stretching and H–O–H bending vibrations in H_2O molecules [45]. At around 1900 nm, all five samples showed strong absorption peaks, likely due to a combination of OH stretching and water bending modes. The peak around 2400 nm was due to the combination of the stretching mode of the SO_4^{2-} tetrahedron and the bending mode of water [38,42]. The detailed assignments of absorption peaks are listed in Table 3.

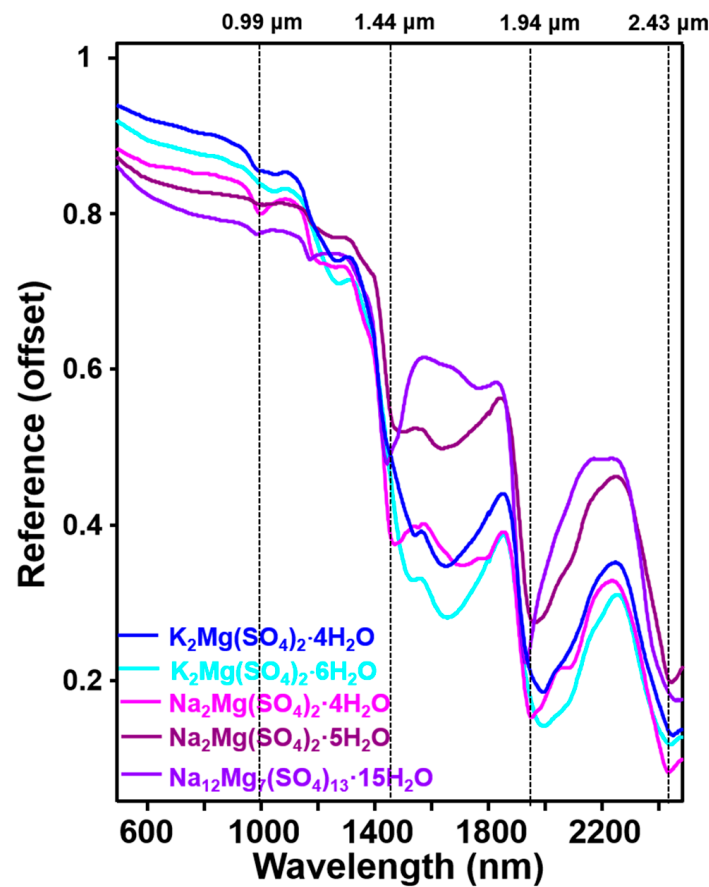


Figure 4. VNIR spectra of five magnesium sulfate double salts. The absorption peaks are mainly caused by water molecules, which can be used to help detect them by CRISM and SWIR on Mars. The samples without water are not distinctive and are not included in the spectra.

Table 3. VNIR peak position (cm^{-1}) and assignment of five hydrous magnesium sulfate double salts.

$\text{K}_2\text{Mg}(\text{SO}_4)_2 \cdot 4\text{H}_2\text{O}$	$\text{K}_2\text{Mg}(\text{SO}_4)_2 \cdot 6\text{H}_2\text{O}$	$\text{Na}_2\text{Mg}(\text{SO}_4)_2 \cdot 4\text{H}_2\text{O}$	$\text{Na}_2\text{Mg}(\text{SO}_4)_2 \cdot 5\text{H}_2\text{O}$	$\text{Na}_{12}\text{Mg}_7(\text{SO}_4)_{13} \cdot 15\text{H}_2\text{O}$	Assignment
990				984	$2\nu_1^W + \nu_2^W$
1051	1040	1000	1000		$3\nu_1^W$ or ν_1^W
				1172	$2\nu_1^W + \nu_2^W$
1268	1273	1263	1265		$\nu_1^W + \nu_2^W + \nu_3^{\text{SO}_4}$
1541	1534	1469	1491	1442	$2\nu_1^W$ or $2\nu_3^W$
1650	1656	1550	1638		$2\nu_1^W$ or $2\nu_3^W$
		1709		1765	$\nu_2^W + \nu_3^W$ (or ν_1^W) + ν_{LT}
		1951	1963	1930	$\nu_1^W + \nu_2^W$ (or ν_3^W)
1993	1994	2080			$\nu_1^W + \nu_2^W$ (or ν_3^W)
				2201	ν_1^W (or ν_3^W) + $\nu_3^{\text{SO}_4}$
2450	2441	2435	2445	2465	$\nu_2^W + \nu_1^{\text{SO}_4} + \nu_3^{\text{SO}_4}$

4. Discussion and Implications for Mars

On Mars, different types of sulfate minerals have been identified by multiple payloads. For example, Ca-sulfates and Mg-sulfates were detected in different elements of the Gale Crater using CheMin (XRD) measurements, and in Jezero Crater in different formations using SHELORC (Raman) measurements. Different species of sulfates were also detected through the IR payloads from the orbiter and in situ rovers, such as PanCam (UV-VNIR) on the Opportunity and Spirit rovers, CRISM on MRO, and OMEGA on Mars Express. However, most sulfates are only inferred to exist on the Martian surface because the spectra shape are similar and there is a lack of reference data. Some minerals synthesized in this study have been detected in Mars-analog environments, such as $\text{Na}_2\text{Mg}(\text{SO}_4)_2 \cdot 4\text{H}_2\text{O}$ and $\text{K}_2\text{Mg}(\text{SO}_4)_2 \cdot 4\text{H}_2\text{O}$, which have been identified in the Atacama desert, one of the most famous Mars-analog sites [46]. This means that $\text{Na}_2\text{Mg}(\text{SO}_4)_2 \cdot 4\text{H}_2\text{O}$, $\text{K}_2\text{Mg}(\text{SO}_4)_2 \cdot 4\text{H}_2\text{O}$, and other minerals synthesized in this study most probably occur on Mars. Therefore, the spectra features obtained in this study can serve as a database for detecting seven different magnesium sulfate double salts.

X-ray diffraction (XRD) serves as a versatile non-destructive analytical technique employed for analyzing various physical properties, including phase composition, crystal structure, and orientation, across powder, solid, and liquid samples. X-ray powder diffraction is now routinely exploited for the identification of minerals in geological materials.

Specifically, CheMin stands out as a miniaturized X-ray diffraction/X-ray fluorescence (XRD/XRF) instrument that is among the ten instruments situated either on or inside the rover, each crafted to furnish comprehensive insights into the rocks, soils, and atmosphere within the designated region. The obtained XRD patterns of the seven synthesized magnesium sulfate double salts will benefit CheMin-based detection in the Gale Crater.

Raman spectroscopy has proven highly valuable in situ for identifying and characterizing mineral phases during planetary surface exploration, encompassing hydrous magnesium sulfates and magnesium sulfate double salts. Our findings indicate that magnesium sulfate double salts exhibit distinct and precise Raman signatures, facilitating direct identification of their phases from raw spectra. This feature promises utility in NASA's Mars2020 mission using SuperCam and SHERLOC instruments, and in future Mars missions like the ExoMars RSL. Additionally, these data aid in distinguishing magnesium sulfate double salts from other minerals like sulfates and chlorides, which are less easily discerned using alternative spectroscopic techniques. FTIR spectroscopy serves as the current standard for acquiring MIR spectra in laboratory settings, exhibiting high sensitivity to both organic and inorganic phases, including hydrous and anhydrous compounds. Leveraging the principles of MIR, a Thermal Emission Imaging System (THEMIS) was developed and deployed on the Mars Global Surveyor and Mars Odyssey orbiters for remote sensing from orbit. Chojnacki et al. utilized THEMIS data to identify the spectral features of magnesium sulfate-bearing materials in Valles Marineris on Mars [47]. The MIR spectra obtained in our study contribute to the characterization of magnesium sulfate double salt-bearing minerals on Mars using thermal emission spectroscopic techniques, specifically data from THEMIS.

VNIR spectroscopy stands out as the most widely employed technique in orbital remote sensing, offering insights even into biological activities. Nevertheless, the spectral bands around 1.4, 1.9, and 2.4 μm in the VNIR spectra of hydrated magnesium sulfate

double salts may overlap with the typical features of certain other hydrated minerals, posing challenges in distinguishing these phases accurately. The standard VNIR spectra we generated for hydrated magnesium sulfate double salts in this study will prove instrumental for VNIR/NIR payload utilization in orbital remote sensing and standoff sensing during forthcoming exploration missions to Mars.

It is true that pure mineral phases are not common in the complex natural systems of Mars. Instead, complex phases are more prevalent, due to the solubilization of salts in soil and rocks triggered by natural processes like groundwater upwelling. This process involves various inorganic compounds, making the composition of the soil and rocks on Mars quite complex. The subsequent vaporization of water leads to the formation of intricate solid mixtures. According to previous studies, evaporite salts (e.g., Na_2SO_4 (thenardite), $\text{Na}_2\text{SO}_4 \cdot 10\text{H}_2\text{O}$ (mirabilite), $\text{MgSO}_4 \cdot 6\text{H}_2\text{O}$ (hexahydrite), $\text{MgSO}_4 \cdot 7\text{H}_2\text{O}$ (epsomite), $\text{Na}_2\text{Mg}(\text{SO}_4)_2 \cdot 4\text{H}_2\text{O}$ (blödite), and $\text{Na}_2\text{Mg}(\text{SO}_4)_2 \cdot 5\text{H}_2\text{O}$ (konyaite)) can be found in saline soil in Mars-analog environments [27,33,48]. Environmental factors can transport these mixtures and minerals to different environment subtypes, such as into the atmosphere, where they are expected to form particles or dissolve and recrystallize into double salts. By analyzing the types and distribution of these produced materials, the sedimentary environments and the environmental factors that produced them can be inferred. Accurate identification of these minerals requires corresponding spectral data; therefore, knowledge of the different spectra properties (e.g., XRD, Raman, MIR, and VNIR) of these mixtures and minerals is essential for analytical purposes.

Evaporite-rich sedimentary deposits on Mars were formed under chemical conditions significantly different from those on Earth. The distinct chemistries of these deposits serve as a record of the chemical and aqueous conditions during their formation and potentially subsequent alterations. During in situ explorations by Mars rovers (e.g., the Opportunity, Spirit, and Curiosity rovers), magnesium sulfate (MgSO_4) salts have been prominently identified, often associated with calcium and iron sulfates, or existing as mixture salts or double salts within the regolith [49–51]. These findings have contributed significantly to understanding the geochemistry of Mars [51,52], indicating the potential presence of high sulfate concentrations in past and/or present Martian brines. Furthermore, magnesium sulfates, as revealed by previous studies [2,51,53], may contribute to the water content in the regolith, underscoring the importance of investigating the interaction among Mg-, Fe-, and Ca-sulfates and water, particularly during dynamic processes such as evaporation.

Although direct detection of magnesium sulfate double salts on Mars has not been achieved, numerical evidence supports the possibility of their occurrence on the planet [14, 19–21,27,28,54]. For example, the in situ detection of magnesium sulfate sedimentary rock associated with calcium sulfates and light-toned veins showed that these structures contain many cations and sulfate ions in different typical regions of Mars, and much modeling has been conducted to understand the evaporation of minerals under Martian conditions [14,19–21,27,28]. All results show support for the existence of magnesium sulfate double salts on Mars. The results of this study not only contribute to the potential detection of magnesium sulfate double salts on Mars, but also offer insights into plausible sulfate formation scenarios. Furthermore, this work enhances our understanding of sulfate formation processes, volcanic activities, and the hydrogeologic settings of typical regions on Mars. For example, the fact that $\text{K}_2\text{CaMg}(\text{SO}_4)_3$ and langbeinite were synthesized at higher temperatures may indicate their presence them around volcanoes, near lava flow areas, and near the impact areas that provide heat sources on Mars. The other five magnesium sulfate double salts can most probably be identified in areas with a geological history of aqueous activities, such as those formed with different fluids, fractures, hydrothermal systems, and other evaporite environments. Moreover, these aqueous solutions may have originated from groundwater upwellings, springs, and hydrothermal fluids formed by the impact process. In summary, both the synthetic methods of magnesium sulfate double salts and their obtained spectroscopic data are of great significance for understanding the geological environment of Mars and its geochemical processes.

5. Conclusions

In this study, seven magnesium sulfate double salts were synthesized in the laboratory, and spectroscopic studies were conducted using XRD, Raman spectroscopy, MIR, and VNIR techniques. The homogeneity and phase of seven samples were determined by XRD patterning. The Raman spectra unveiled the molecular fundamental vibrational modes, with the ν_1 mode of SO_4^{2-} being particularly prominent. To complement the Raman data and reveal additional fundamental vibrational modes, MIR spectra were collected. Additionally, VNIR spectra were acquired to expose the combination modes of water and the SO_4^{2-} tetrahedron. Different samples showed unique spectra features that can be used to precisely identify phases in evaporite environments on Earth and Mars. Raman spectroscopy, in particular, can easily distinguish samples with the same cations but different hydrated states, and samples with different cations. These data will be helpful for data processing in instruments used in Mars exploration with the same spectrum (e.g., RLS at Oxia Planum and SHERLOC at the Jezero Crater), and the features of Raman, MIR, and VNIR can assist in the identification of Martian sulfates and aid in understanding environmental changes on Mars and Earth. In general, both the synthesis methods of magnesium sulfate double salts and the spectral data obtained from them are of significant importance for understanding the geological environment and geochemical processes of Mars.

Author Contributions: Methodology, E.S. and Y.X.; experiment, R.Z.; data analysis and writing—original draft preparation, R.Z. and E.S.; writing—review and editing, Y.X., E.S., X.Z. and E.J.; formal analysis, X.Z. and E.J.; supervision, Y.X.; project administration, Y.X. and E.S.; funding acquisition, Z.L. All authors have read and agreed to the published version of the manuscript.

Funding: This work was funded by the National Natural Science Foundation of China (Nos. U1931211 and 41972322), Natural Science Foundation of Shandong Province (ZR2023QD157), China Postdoctoral Science Foundation (2022M721916), and Pre-research project on Civil Aerospace Technologies funded by the China National Space Administration (No. D020102).

Data Availability Statement: The digital file corresponding to the spectral data in the figures of this manuscript is available (Shi and Zhang et al. (2024)) [55]. No user ID and password are required to access these data. <https://doi.org/10.6084/m9.figshare.24999287.v2> accessed on 15 January 2024.

Acknowledgments: This work was also supported by the Physical-Chemical Materials Analytical and Testing Center of Shandong University at Weihai.

Conflicts of Interest: The authors declare no conflicts of interest.

References

1. Baird, A.K.; Toulmin, P.; Clark, B.C.; Rose, H.J.; Keil, K.; Christian, R.P.; Gooding, J.L. Mineralogic and Petrologic Implications of Viking Geochemical Results from Mars: Interim Report. *Science* **1976**, *194*, 1288–1293. [CrossRef]
2. Vaniman, D.T.; Bish, D.L.; Chipera, S.J.; Fialips, C.I.; William Carey, J.; Feldman, W.C. Magnesium Sulphate Salts and the History of Water on Mars. *Nature* **2004**, *431*, 663–665. [CrossRef]
3. Di Pietro, I.; Schmidt, G.; Tangari, A.C.; Salese, F.; Silvestro, S.; Fairén, A.G.; Marinangeli, L.; Pondrelli, M. Groundwater-Controlled Deposition of Equatorial Layered Deposits in Central Arabia Terra, Mars. *JGR Planets* **2023**, *128*, e2022JE007504. [CrossRef]
4. Arvidson, R.E.; Poulet, F.; Bibring, J.-P.; Wolff, M.; Gendrin, A.; Morris, R.V.; Freeman, J.J.; Langevin, Y.; Mangold, N.; Bellucci, G. Spectral Reflectance and Morphologic Correlations in Eastern Terra Meridiani, Mars. *Science* **2005**, *307*, 1591–1594. [CrossRef]
5. Gendrin, A.; Mangold, N.; Bibring, J.-P.; Langevin, Y.; Gondet, B.; Poulet, F.; Bonello, G.; Quantin, C.; Mustard, J.; Arvidson, R.; et al. Sulfates in Martian Layered Terrains: The OMEGA/Mars Express View. *Science* **2005**, *307*, 1587–1591. [CrossRef]
6. Peterson, R.C.; Wang, R. Crystal Molds on Mars: Melting of a Possible New Mineral Species to Create Martian Chaotic Terrain. *Geology* **2006**, *34*, 957. [CrossRef]
7. Mangold, N.; Gendrin, A.; Gondet, B.; LeMouelic, S.; Quantin, C.; Ansan, V.; Bibring, J.-P.; Langevin, Y.; Masson, P.; Neukum, G. Spectral and Geological Study of the Sulfate-Rich Region of West Candor Chasma, Mars. *Icarus* **2008**, *194*, 519–543. [CrossRef]
8. Roach, L.H.; Mustard, J.F.; Murchie, S.L.; Bibring, J.-P.; Forget, F.; Lewis, K.W.; Aharonson, O.; Vincendon, M.; Bishop, J.L. Testing Evidence of Recent Hydration State Change in Sulfates on Mars. *J. Geophys. Res.* **2009**, *114*, 2008JE003245. [CrossRef]
9. Wendt, L.; Gross, C.; Kneissl, T.; Sowe, M.; Combe, J.-P.; LeDeit, L.; McGuire, P.C.; Neukum, G. Sulfates and Iron Oxides in Ophir Chasma, Mars, Based on OMEGA and CRISM Observations. *Icarus* **2011**, *213*, 86–103. [CrossRef]

10. Liu, Y.; Goudge, T.A.; Catalano, J.G.; Wang, A. Spectral and Stratigraphic Mapping of Hydrated Minerals Associated with Interior Layered Deposits near the Southern Wall of Melas Chasma, Mars. *Icarus* **2018**, *302*, 62–79. [[CrossRef](#)]
11. Sheppard, R.Y.; Thorpe, M.T.; Fraeman, A.A.; Fox, V.K.; Milliken, R.E. Merging Perspectives on Secondary Minerals on Mars: A Review of Ancient Water-Rock Interactions in Gale Crater Inferred from Orbital and In-Situ Observations. *Minerals* **2021**, *11*, 986. [[CrossRef](#)]
12. Christensen, P.R.; Wyatt, M.B.; Glotch, T.D.; Rogers, A.D.; Anwar, S.; Arvidson, R.E.; Bandfield, J.L.; Blaney, D.L.; Budney, C.; Calvin, W.M.; et al. Mineralogy at Meridiani Planum from the Mini-TES Experiment on the Opportunity Rover. *Science* **2004**, *306*, 1733–1739. [[CrossRef](#)]
13. Arvidson, R.E.; Squyres, S.W.; Anderson, R.C.; Bell, J.F.; Blaney, D.; Brückner, J.; Cabrol, N.A.; Calvin, W.M.; Carr, M.H.; Christensen, P.R.; et al. Overview of the Spirit Mars Exploration Rover Mission to Gusev Crater: Landing Site to Backstay Rock in the Columbia Hills. *J. Geophys. Res.* **2006**, *111*, 2005JE002499. [[CrossRef](#)]
14. Rapin, W.; Ehlmann, B.L.; Dromart, G.; Schieber, J.; Thomas, N.H.; Fischer, W.W.; Fox, V.K.; Stein, N.T.; Nachon, M.; Clark, B.C.; et al. An Interval of High Salinity in Ancient Gale Crater Lake on Mars. *Nat. Geosci.* **2019**, *12*, 889–895. [[CrossRef](#)]
15. Chipera, S.J.; Vaniman, D.T.; Rampe, E.B.; Bristow, T.F.; Martínez, G.; Tu, V.M.; Peretyazhko, T.S.; Yen, A.S.; Gellert, R.; Berger, J.A.; et al. Mineralogical Investigation of Mg-Sulfate at the Canaima Drill Site, Gale Crater, Mars. *JGR Planets* **2023**, *128*, e2023JE008041. [[CrossRef](#)]
16. Vaniman, D.T.; Chipera, S.J. Transformations of Mg- and Ca-Sulfate Hydrates in Mars Regolith. *Am. Mineral.* **2006**, *91*, 1628–1642. [[CrossRef](#)]
17. Rapin, W.; Dromart, G.; Clark, B.C.; Schieber, J.; Kite, E.S.; Kah, L.C.; Thompson, L.M.; Gasnault, O.; Lasue, J.; Meslin, P.-Y.; et al. Sustained Wet–Dry Cycling on Early Mars. *Nature* **2023**, *620*, 299–302. [[CrossRef](#)] [[PubMed](#)]
18. Arvidson, R.E.; Squyres, S.W.; Bell, J.F.; Catalano, J.G.; Clark, B.C.; Crumpler, L.S.; De Souza, P.A.; Fairén, A.G.; Farrand, W.H.; Fox, V.K.; et al. Ancient Aqueous Environments at Endeavour Crater, Mars. *Science* **2014**, *343*, 1248097. [[CrossRef](#)] [[PubMed](#)]
19. Rapin, W.; Meslin, P.-Y.; Maurice, S.; Vaniman, D.; Nachon, M.; Mangold, N.; Schröder, S.; Gasnault, O.; Forni, O.; Wiens, R.C.; et al. Hydration State of Calcium Sulfates in Gale Crater, Mars: Identification of Bassanite Veins. *Earth Planet. Sci. Lett.* **2016**, *452*, 197–205. [[CrossRef](#)]
20. Nachon, M.; Clegg, S.M.; Mangold, N.; Schröder, S.; Kah, L.C.; Dromart, G.; Ollila, A.; Johnson, J.R.; Oehler, D.Z.; Bridges, J.C.; et al. Calcium Sulfate Veins Characterized by ChemCam/Curiosity at Gale Crater, Mars. *JGR Planets* **2014**, *119*, 1991–2016. [[CrossRef](#)]
21. Nachon, M.; López-Reyes, G.; Meslin, P.-Y.; Ollila, A.M.; Mandon, L.; Clavé, E.; Forni, O.; Maurice, S.; Wiens, R.C.; Gasnault, O.; et al. Light-Toned Veins and Material in Jezero Crater, Mars, as Seen In-Situ via NASA’s Perseverance Rover (Mars 2020 Mission): Stratigraphic Distribution and Compositional Results. In Proceedings of the LPSC 2024-55th Lunar and Planetary Science Conference, Woodlands, TX, USA, 11–15 March 2023.
22. Yen, A.S.; Ming, D.W.; Vaniman, D.T.; Gellert, R.; Blake, D.F.; Morris, R.V.; Morrison, S.M.; Bristow, T.F.; Chipera, S.J.; Edgett, K.S.; et al. Multiple Stages of Aqueous Alteration along Fractures in Mudstone and Sandstone Strata in Gale Crater, Mars. *Earth Planet. Sci. Lett.* **2017**, *471*, 186–198. [[CrossRef](#)]
23. Clark, B.C.; Morris, R.V.; McLennan, S.M.; Gellert, R.; Jolliff, B.; Knoll, A.H.; Squyres, S.W.; Lowenstein, T.K.; Ming, D.W.; Tosca, N.J.; et al. Chemistry and Mineralogy of Outcrops at Meridiani Planum. *Earth Planet. Sci. Lett.* **2005**, *240*, 73–94. [[CrossRef](#)]
24. Banin, A.; Han, F.X.; Kan, I.; Cicelsky, A. Acidic Volatiles and the Mars Soil. *J. Geophys. Res.* **1997**, *102*, 13341–13356. [[CrossRef](#)]
25. Catling, D.C. A Chemical Model for Evaporites on Early Mars: Possible Sedimentary Tracers of the Early Climate and Implications for Exploration. *J. Geophys. Res.* **1999**, *104*, 16453–16469. [[CrossRef](#)]
26. Newsom, H.E.; Hagerty, J.J.; Goff, F. Mixed Hydrothermal Fluids and the Origin of the Martian Soil. *J. Geophys. Res.* **1999**, *104*, 8717–8728. [[CrossRef](#)]
27. King, P.L.; Lescinsky, D.T.; Nesbitt, H.W. The Composition and Evolution of Primordial Solutions on Mars, with Application to Other Planetary Bodies. *Geochim. Cosmochim. Acta* **2004**, *68*, 4993–5008. [[CrossRef](#)]
28. Al-Samir, M.; Nabhan, S.; Winkler, A.; Fritz, J.; Greshake, A.; Jaumann, R. Experimental Leaching Processes and the Formation of Sulfates with Sulfuric Acid on Terrestrial Rocks, Martian-Like Rocks and the Martian Meteorite Tissint Related to the Formation of ILD’s on Mars. In Proceedings of the 44th Annual Lunar and Planetary Science Conference, Woodlands, TX, USA, 18–22 March 2013.
29. Noel, A.; Bishop, J.L.; Al-Samir, M.; Gross, C.; Flahaut, J.; McGuire, P.C.; Weitz, C.M.; Seelos, F.; Murchie, S. Mineralogy, Morphology and Stratigraphy of the Light-Toned Interior Layered Deposits at Juventae Chasma. *Icarus* **2015**, *251*, 315–331. [[CrossRef](#)]
30. Kite, E.S.; Melwani Daswani, M. Geochemistry Constrains Global Hydrology on Early Mars. *Earth Planet. Sci. Lett.* **2019**, *524*, 115718. [[CrossRef](#)]
31. Gutierrez, A.; Ushak, S.; Mamani, V.; Vargas, P.; Barreneche, C.; Cabeza, L.F.; Grágeda, M. Characterization of Wastes Based on Inorganic Double Salt Hydrates as Potential Thermal Energy Storage Materials. *Sol. Energy Mater. Sol. Cells* **2017**, *170*, 149–159. [[CrossRef](#)]
32. Ait Ousaleh, H.; Sair, S.; Zaki, A.; Faik, A.; Mirena Igartua, J.; El Bouari, A. Double Hydrates Salt as Sustainable Thermochemical Energy Storage Materials: Evaluation of Dehydration Behavior and Structural Phase Transition Reversibility. *Sol. Energy* **2020**, *201*, 846–856. [[CrossRef](#)]

33. Vargas Jentzsch, P.; Kampe, B.; Rösch, P.; Popp, J. Raman Spectroscopic Study of Crystallization from Solutions Containing MgSO_4 and Na_2SO_4 : Raman Spectra of Double Salts. *J. Phys. Chem. A* **2011**, *115*, 5540–5546. [[CrossRef](#)] [[PubMed](#)]
34. Souamti, A.; Chehimi, D.B.H. Effects of Gd_2O_3 Doping on the Structure and the Conduction Mechanism of $\text{K}_2\text{Mg}_2(\text{SO}_4)_3$ Langbeinite Ceramics: A Comparative Study. *Mater. Sci. Eng. B* **2021**, *265*, 115040. [[CrossRef](#)]
35. Hertweck, B.; Giester, G.; Libowitzky, E. The Crystal Structures of the Low-Temperature Phases of Leonite-Type Compounds, $\text{K}_2\text{Me}(\text{SO}_4)_2 \cdot 4\text{H}_2\text{O}$ ($\text{Me}^{2+} = \text{Mg}, \text{Mn}, \text{Fe}$). *Am. Miner.* **2001**, *86*, 1282–1292. [[CrossRef](#)]
36. Dhandapani, M.; Thyagu, L.; Prakash, P.A.; Amirthaganesan, G.; Kandhaswamy, M.A.; Srinivasan, V. Synthesis and Characterization of Potassium Magnesium Sulphate Hexahydrate Crystals. *Cryst. Res. Technol.* **2006**, *41*, 328–331. [[CrossRef](#)]
37. Gates-Rector, S.; Blanton, T. The Powder Diffraction File: A Quality Materials Characterization Database. *Powder Diffr.* **2019**, *34*, 352–360. [[CrossRef](#)]
38. Ling, Z.C.; Wang, A. A Systematic Spectroscopic Study of Eight Hydrated Ferric Sulfates Relevant to Mars. *Icarus* **2010**, *209*, 422–433. [[CrossRef](#)]
39. Shi, E.; Wang, A.; Ling, Z. MIR, VNIR, NIR, and Raman Spectra of Magnesium Chlorides with Six Hydration Degrees: Implication for Mars and Europa. *J. Raman Spectrosc.* **2020**, *51*, 1589–1602. [[CrossRef](#)]
40. Shi, E.; Zeng, X.; Chen, J.; Ling, Z. Spectroscopic Analysis of Ca-Sr Sulfate Solid Solutions for In-Situ Observations on Mars. *LPI Contrib.* **2024**, *3040*, 1794.
41. Marzougui, H.; Martin, I.R.; Attia-Essaies, S.; Hassen-Chehimi, D.B.; Lalla, E.; Léon-Luis, S.F. Site Selective Luminescence of Eu^{3+} Ions in $\text{K}_2\text{Mg}(\text{SO}_4)_2 \cdot 6\text{H}_2\text{O}$ Crystal. *Opt. Mater.* **2015**, *46*, 339–344. [[CrossRef](#)]
42. Ju, E.; Shi, E.; Xin, Y.; Cao, H.; Liu, C.; Liu, P.; Chen, J.; Fu, X.; Ling, Z. Laboratory Synthesis, Spectroscopic Characteristics, and Conversion Relationships of Five Calcium Sulfate Double Salts Relevant to Mars. *Icarus* **2023**, *401*, 115610. [[CrossRef](#)]
43. Cloutis, E.; Hawthorne, F.; Mertzman, S.; Krenn, K.; Craig, M.; Marcino, D.; Methot, M.; Strong, J.; Mustard, J.; Blaney, D. Detection and Discrimination of Sulfate Minerals Using Reflectance Spectroscopy. *Icarus* **2006**, *184*, 121–157. [[CrossRef](#)]
44. Mikhailov, M.M.; Yuryev, S.A.; Lapin, A.N. Investigating Changes in the Diffuse Reflectance Spectra of BaSO_4 Powders Modified with SiO_2 Nanoparticles Exposed to Proton Irradiation. *Nucl. Instrum. Methods Phys. Res. Sect. B Beam Interact. Mater. At.* **2023**, *539*, 62–67. [[CrossRef](#)]
45. De Angelis, S.; Carli, C.; Tosi, F.; Beck, P.; Schmitt, B.; Piccioni, G.; De Sanctis, M.C.; Capaccioni, F.; Di Iorio, T.; Philippe, S. Temperature-Dependent VNIR Spectroscopy of Hydrated Mg-Sulfates. *Icarus* **2017**, *281*, 444–458. [[CrossRef](#)]
46. De Waele, J.; Carbone, C.; Sanna, L.; Vattano, M.; Galli, E.; Sauro, F.; Forti, P. Secondary Minerals from Salt Caves in the Atacama Desert (Chile): A Hyperarid and Hypersaline Environment with Potential Analogies to the Martian Subsurface. *Int. J. Speleol.* **2017**, *46*, 51–66. [[CrossRef](#)]
47. Chojnacki, M.; Hynek, B.M. Geological Context of Water-altered Minerals in Valles Marineris, Mars. *J. Geophys. Res.* **2008**, *113*, 2007JE003070. [[CrossRef](#)]
48. Hughes, E.B.; Gilmore, M.S.; Martin, P.E.; Eleazer, M. Visible to Near-Infrared Reflectance and Raman Spectra of Evaporites from Sulfate-Chloride Mars Analogue Brines. *Icarus* **2023**, *401*, 115597. [[CrossRef](#)]
49. Lane, M.D.; Dyar, M.D.; Bishop, J.L. Spectroscopic Evidence for Hydrated Iron Sulfate in the Martian Soil. *Geophys. Res. Lett.* **2004**, *31*, 2004GL021231. [[CrossRef](#)]
50. Altheide, T.; Chevrier, V.; Nicholson, C.; Denson, J. Experimental Investigation of the Stability and Evaporation of Sulfate and Chloride Brines on Mars. *Earth Planet. Sci. Lett.* **2009**, *282*, 69–78. [[CrossRef](#)]
51. Moore, J.M.; Bullock, M.A.; Newsom, H.; Nelson, M. Laboratory Simulations of Mars Evaporite Geochemistry. *J. Geophys. Res.* **2010**, *115*, 2008JE003208. [[CrossRef](#)]
52. Tosca, N.J.; McLennan, S.M.; Dyar, M.D.; Sklute, E.C.; Michel, F.M. Fe Oxidation Processes at Meridiani Planum and Implications for Secondary Fe Mineralogy on Mars. *J. Geophys. Res.* **2008**, *113*, 2007JE003019. [[CrossRef](#)]
53. Chou, I.; Seal, R.R. Magnesium and Calcium Sulfate Stabilities and the Water Budget of Mars. *J. Geophys. Res.* **2007**, *112*, 2007JE002898. [[CrossRef](#)]
54. García-Florentino, C.; Gomez-Nubla, L.; Huidobro, J.; Torre-Fdez, I.; Ruíz-Galende, P.; Aramendia, J.; Hausrath, E.M.; Castro, K.; Arana, G.; Madariaga, J.M. Interrelationships in the Gypsum–Syngenite–Görgeyite System and Their Possible Formation on Mars. *Astrobiology* **2021**, *21*, 332–344. [[CrossRef](#)] [[PubMed](#)]
55. Zhang, R.; Shi, E.; Zeng, X.; Ju, E.; Ling, Z. Spectroscopies of Magnesium Sulfate Double Salts and Their Implication for Mars. 2024. Available online: https://figshare.com/articles/dataset/_b_Spectroscopies_of_magnesium_sulfate_double_salts_and_their_implication_for_Mars_b_/24999287 (accessed on 27 April 2024).

Disclaimer/Publisher’s Note: The statements, opinions and data contained in all publications are solely those of the individual author(s) and contributor(s) and not of MDPI and/or the editor(s). MDPI and/or the editor(s) disclaim responsibility for any injury to people or property resulting from any ideas, methods, instructions or products referred to in the content.